Journal of Alloys and Compounds 586 (2014) S469–S471

Contents lists available at SciVerse ScienceDirect

Journal of Alloys and Compounds

journal homepage: www.elsevier.com/locate/jalcom

X-ray studies of nanostructured Ti_2NiCu shape memory alloy

P. Ari-Gur [a,*], A.S.B. Madiligama [a], S.G. Watza [a], A. Shelyakov [b], D. Kuchin [c], V. Koledov [c], W. Gao [d]

[a] Western Michigan University, Kalamazoo, MI, USA
[b] National Research Nuclear University, Moscow Engineering Physics Institute, Kashirskoesh., 31, Moscow 115409, Russia
[c] Kotelnikov Institute of Radio Engineering and Electronics, RAS, Moscow 125009, Russia
[d] Department of Chemical and Materials Engineering, University of Auckland, New Zealand

ARTICLE INFO

Article history:
Available online 23 January 2013

Keywords:
Crystallographic texture
Nitinol
Shape memory
Ti–Ni–Cu

ABSTRACT

Phase-mix, phase transformations and crystallographic texture of amorphous/nanostructure melt-spun ribbons of Ti_2NiCu were studied using X-ray diffraction and nano-indentation. Their peak two-way shape-memory effect occurs when most of the austenite (cubic, B2) phase has converted to martensite (orthorhombic, B19), but before grain growth takes place. The melt-spinning process imparts strong B2 {100} texture that is retained as B19 (100) and (011) after phase transition during subsequent annealing. Because the phase transformation and texture strongly depend on the annealing process, it should be possible to tailor them for further improving their performance.

1. Introduction

Nitinol and related alloys exhibit two extraordinary, closely-related properties: shape memory effect (SME) and superelasticity. When these alloys are nanostructured, they demonstrate outstanding strength and reliability [1]. Nanostructured NiTi produced from coarse grained one by severe plastic deformation (SPD) technique is significantly stronger, more reliable and provides larger counterforce than traditional Nitinol [2]. Ti_2NiCu rapidly-quenched alloys are of particular interest for application in MEMS technology because of their perfect SME, narrow hysteresis and high reliability [3]. Recently the nanostructured Ti_2NiCu alloy have been produced by entirely different technique – controlled annealing from amorphous state (CAAS) and applied to design of record small nano-tweezers [4–9]. The key to the performance of shape-memory alloys is their crystalline structure and the orientation relationship between the austenite and martensite; hence, the understanding of the effect of processing on the structure is critical for optimizing properties.

2. Background

Copper, replacing some of the nickel atoms in Nitinol, causes the martensitic transformation temperature to increase. Copper also improves the corrosion resistance of the alloy, results in narrow hysteresis and prevents the formation of Ti_3Ni_4 precipitates [9–11], all are beneficial properties. The crystalline structure of the final martensitic phase, as well as that of the intermediate phases, strongly depends on the amount of copper in the alloy. Above 15% Cu the martensitic structure of bulk Ti_2NiCu is orthorhombic B19 [12].

The technology used to prepare the alloy and subsequent heat treatments, have a strong effect on the crystalline structure and the nature of phase transformation. Non-conventional casting techniques (such as melt spinning) are increasingly used for the production of shape memory alloys with desirable properties [13].

The shape memory feature of Nitinol-based alloys is affected by the stress-induced martensitic transformation. The nature of the crystallographic texture plays, then, a key role in the mechanical properties of the alloy. The texture that develops in Ti_2NiCu depends strongly on the geometrical shape of the part as well as on the processing parameters [14–16]. It is essential to study the character of the crystallographic texture and to try to control it for maximum performance.

3. Materials and methods

Melt-spun ribbons of Ti_2NiCu were prepared by very rapid quenching. They were 40 μm thick and 1.8 mm wide. Then the as-spun ribbons were treated by CAAS technique. They were annealed by passing *pulses* of electric current through the ribbon. The electric pulse causes the ribbon temperature to rise. When it reaches the T_{cr} value, the crystallization process starts and continues till the pulse ends. Because the resistance (R) of crystalline ribbons, R_{cr}, is smaller than that of amorphous ones, R_a, the crystallization process under current can be controlled by measuring the resistance R of the sample.

The fraction of the crystalline phase can be *approximated* by $r = (R_a - R)/(R_a - R_{cr}) * 100\%$. Samples were chosen with r values in the range between 0 (as-spun ribbon) and 96% ('almost fully crystallized').

More details of sample preparation are given elsewhere [5].

4. Experimental procedure

Recoverable strain was measured in bending. The samples were deformed in bending in the martensite state with the use of glass

* Corresponding author.
E-mail address: pnina.ari-gur@wmich.edu (P. Ari-Gur).

0925-8388/$ - see front matter © 2013 Elsevier B.V. All rights reserved.
http://dx.doi.org/10.1016/j.jallcom.2012.12.109

cylinder of 3 mm in diameter. The temperature was then changed in cycles to determine shape recovery due to SME.

X-ray diffraction scans were conducted on each side of the ribbon using Philips vertical goniometer with Cu Kα radiation (λ = 0.1541 nm). The penetration in these alloys is about 8 μm and therefore each side represents about 20% of the ribbon (to a total of 40%).

Nano-indentation tests, using MTS XP Nanoindenter, were conducted on the cross section of the samples. For each sample, three positions were tested. The results were compared to DSC tests that were used to study the martensitic transition.

5. Results and discussion

After the thermal cycles, the samples partially or almost fully recovered to their initial shape. The remarkable fact was that some of the samples curved again after cooling to below the martensite transformation. That means that a manifestation of two-way shape memory effect (TWSME) was observed. The recoverable deformation $\Delta\varepsilon$ was calculated as the difference between bending deformation in martensite and austenite. $\Delta\varepsilon$ versus the *approximate* fraction of the crystalline phase r (based on resistance) is given in Table 1.

The air-side X-ray diffraction results of the as-quenched sample (Fig. 1) show that although the bulk of the ribbon is almost entirely amorphous at this condition (as determined by the resistance R), a thin layer close to the surface is crystalline that is almost entirely B2 (austenite) phase with lattice constant $a = 0.3040$ nm. The phase is highly-textured with the {100} plane parallel to the ribbon surface, as is evident from the absence of all other peaks. This is different than the texture found in bulk Ti_2NiCu where the room temperature phase is martensite; this structure results from the very rapid quenching. Considering the sensitivity of the developing texture to sample geometry and processing parameters [14] this result is reasonable. This sample contains also small amount of orthorhombic (B19) phase with lattice constants $a = 0.2914$ nm; $b = 0.4284$ nm; $c = 0.4515$ nm. The martensite of $Ti_2Ni_{1-x}Cu_x$ when $x > 0.15$ is known to be orthorhombic. The B19 phase is also textured with (011) and (100) planes parallel to the surface. Considering the martensitic transformation takes place by shear of the cubic phase, this preferred orientation relationship is not surprising.

X-ray diffraction scans of the air-side of annealed ribbons with a range of amorphous to crystalline (r) ratios shown in Fig. 2. Phase transformation from austenite (B2) to martensite (B19) starts even with slight annealing and occurs in one step (i.e. there is no B19' intermediate phase); the crystallographic textures of the austenite {100} and of the evolving martensitic phase (B19) with the (011) and (100) planes, remain strong. For samples with $r > 0.60$ the amount of B2 diminishes and the structure is that of textured martensite (B19). At this stage the TWSME performance is best, until grain growth starts at high r values.

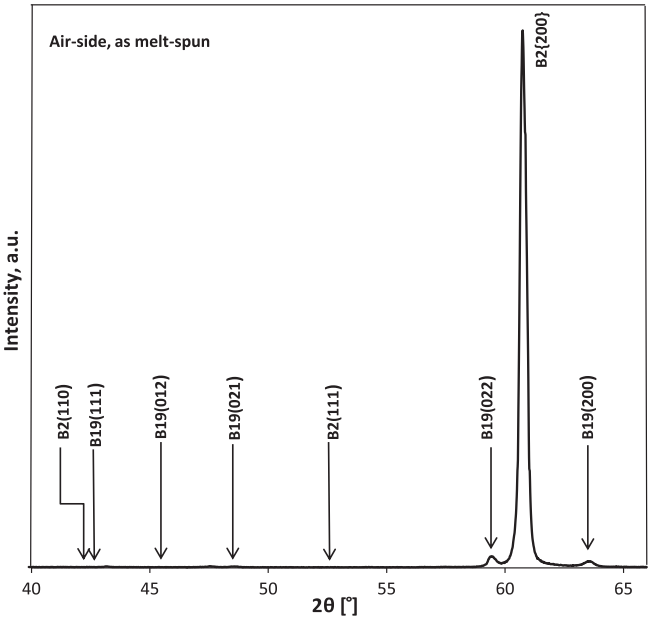

Fig. 1. X-ray scan of the air-side for an as-quenched sample.

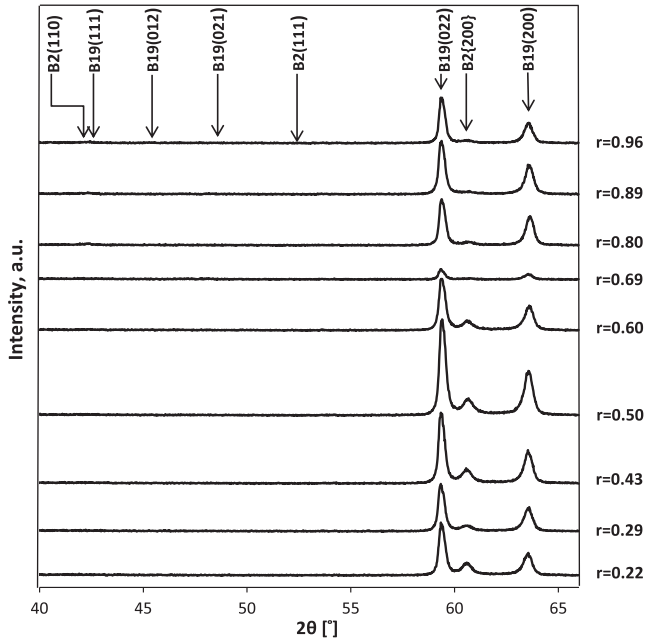

Fig. 2. X-ray scans of the air-side for different r values.

Table 1
The recoverable deformation $\Delta\varepsilon$ induced by TWSME vs. r.

r (%) (*approximate* fraction of crystalline phase)	$\Delta\varepsilon$ (%)
96	0
89	0
80	Close to 0
69	<0.8
63	0.8
60	0.8
29	0
22	0
0	0

X-ray diffraction scans of the wheel-side of ribbons with different annealing conditions are shown in Fig. 3. The as-cast sample is essentially amorphous. Then B2 phase crystallizes from the amorphous bulk. Subsequent annealing results in close to entire phase transformation to B19 (orthorhombic).

The results of nano-indentation performed on the cross-section of the ribbons are shown in Fig. 4. It is known that in these alloys, the martensite is much softer than the austenite so the observed drop in hardness is associated with the increase in B19 concentration and diminishing amounts of B2. The results also coincide well with DSC measurements that are also shown in the figure.

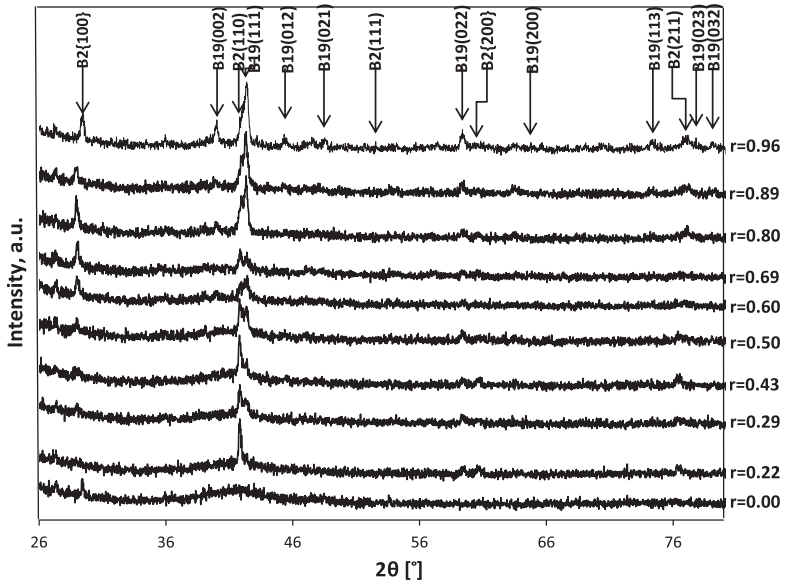

Fig. 3. X-ray scans of the wheel-side for different *r* values.

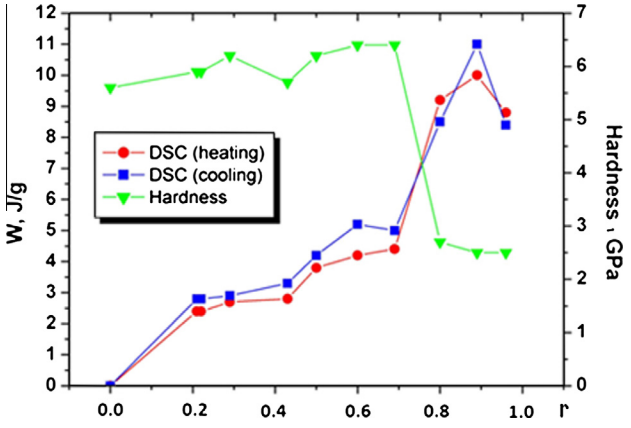

Fig. 4. Nano-indentation of the cross-section of the samples. The martensite is much softer and the drop in hardness is interpreted as the increase in B19 concentration. The results also correlate well with DSC measurements (*W* – thermal energy per one gram, extracted on cooling or absorbed on heating).

6. Conclusions

1. The process of melt-spinning is strongly inhomogeneous and results in a mixed amorphous–crystalline structure of ribbons that is highly textured.
2. The first phase to crystallize is austenite (cubic) B2.
3. The transformation to martensite (orthorhombic) B19 is direct (i.e. occurs in one-step with no intermediate phases formation).
4. When most (but not all) of the ribbon has transformed to martensite, the TWSME performance is best.
5. On the air-side both austenite and martensite display a strong texture, with the B2 {1 0 0} and B19 (1 0 0) and (0 1 1) are parallel to the surface of the ribbon.

Acknowledgments

This work was supported by NSF award No. 0831951, FRACAA award No. 08-050, RFBR-CRDF award No. 11-08-92504 (CRDF award No. RUP1-7028-MO-11).

References

[1] R.Z. Valiev, R.K. Islamgaliev, I.V. Alexandrov, Prog. Mater. Sci. 45 (2000) 103–189.
[2] V.G. Pushin, V.V. Stolyarov, R.Z. Valiev, N.I. Kourov, N.N. Kuranova, E.A. Prokofiev, L.I. Yurchenko, Ann. Chim. Sci. Mat. 27 (2002) 77–88.
[3] N.M. Matveeva, V.G. Pushin, A.V. Shelyakov, Y.U. Bykovskiy, S.B. Volkova, V.S. Kraposhin, Phys. Met. Metallogr. 83 (1997) 626–632.
[4] N. Resnina, S. Belyaev, A. Shelyakov, Eur. Phys. J. Special Top. 158 (2008) 21–26.
[5] A.V. Shelyakov, N.N. Sitnikov, A.P. Menushenkov, A.A. Korneev, R.N. Rizakhanov, N.A. Sokolova, J. Alloys Compd. (2012), in press, http://dx.doi.org/10.1016/j.jallcom.2012.02.146.
[6] S.P. Belyaev, V.V. Istomin-Kastrovskiy, V.V. Koledov, D.S. Kuchin, N.N. Resnina, V.G. Shavrov, A.V. Shelyakov, S.E. Ivanov, Phys. Procedia 10 (2010) 39–43.
[7] D. Zakharov, G. Lebedev, A. Irzhak, V. Afonina, A. Mashirov, V. Kalashnikov, V. Koledov, A. Shelyakov, D. Podgorny, N. Tabachkova, V. Shavrov, Smart Mater. Struct. 21 (2012) 052001, in press, http://dx.doi.org/10.1088/0964-1726/21/5/052001.
[8] A.V. Shelyakov, N.N. Sitnikov, A.P. Menushenkov, V.V. Koledov, A.I. Irjak, Thin Solid Films 519 (2011) 5314–5317.
[9] A.V. Shelyakov, N.N. Sitnikov, V.V. Koledov, D.S. Kuchin, A.I. Irzhak, N. Tabachkova, Int. J. Smart Nano Mater. 2 (2011) 68–77.
[10] F. Fukuda, T. Kakeshita, M. Kitayama, K. Saburi, J. Phys. IV 5 (1995) 714–717.
[11] T.H. Nam, T. Saburi, Y. Nakata, K. Shimizu, Mater. Trans. 31 (1990) 1050–1056.
[12] F.J.J. van Loo, G.F. Bastin, A.J.H. Leenen, J. Alloys Compd. 57 (1978) 111–121.
[13] T. Goryczka, J. Van Humbeeck, Int. J. Mater. Prod. Technol. 33 (2008) 252–264.
[14] S.W. Robertson, V. Imbeni, H.R. Wenk, R.O. Ritchie, J. Biomed. Mater. Res. A 72 (2005) 190–199.
[15] M. Fonte, A. Saigal, Scr. Mater. 63 (2010) 320–323.
[16] X. Gao, D.W. Brown, L.C. Brinson, Proc. SPIE Int. Soc. Opt. Eng. 5764 (2005) 715–726.